Additional and canonical phonon modes in $Hg_{1-x}Cd_xTe(0.06 \leq x \leq 0.7)$

J. Polit, E. M. Sheregii,* and J. Cebulski
Institute of Physics, University of Rzeszów, Rejtana 16a, Rzeszów 35-310, Poland

A. Kisiel
Institute of Physics, Jagiellonian University, Reymonta 4, Kraków 30-059, Poland

B. V. Robouch and A. Marcelli
INFN–Laboratori Nazionali di Frascati, Via E. Fermi 40, I-00044 Frascati, Italy

A. Mycielski
Institute of Physics, Polish Academy of Science, Al. Lotników 32/46, Warsaw, Poland
(Received 15 April 2010; published 30 July 2010)

In this experimental work a conception of the phonon spectra of the $Hg_{1-x}Cd_xTe(x=0.06-0.7)$ solid solution is presented which explains the presence of additional lines in the region 100–115 cm^{-1}. Data of the optical reflectivity measurements obtained in far and middle infrared regions for eleven compositions of these alloys in the temperature range from 20 to 293 K using the synchrotron radiation (DAΦNE-LIGHT in LNF, Italy) as source are analyzed. Analyses were performed on samples of different types (*n* and *p* type) of conductivity as well as the temperature dependences of the line intensity under consideration in the region from 70 to 118 cm^{-1}. The model of two valley potential of the mercury atom in the $Hg_{1-x}Cd_xTe$ lattice is used for interpretation of the additional phonon modes.

DOI: 10.1103/PhysRevB.82.014306 PACS number(s): 63.20.kd, 78.66.Hf

I. INTRODUCTION

It is well known that $Hg_{1-x}Cd_xTe$ (MCT) is a very important material, not only for applications but also as a modeling material for theoretical considerations because the energy gap changes continuously from 0 eV (with $x=0.16$ at 4.2 K) to 1.6 eV (with $x=1$) passing through the singularity point where the inversion of the band structure occurs. The MCT is still the main material for infrared devices, mainly for 8–12 μm wavelengths. Additionally, the $Hg_{1-x}Cd_xTe$ quantum wells look promising for the high efficient infrared detectors and microelectronic devices. The problems relating to the electron structure of $Hg_{1-x}Cd_xTe$ is to stay sufficiently clarified. It does not concern the phonon spectra. Recent work[1] concludes a series of a systematic re-examination of the phonon mode behavior of leading zinc-blend semiconductor alloys in the traditional virtual crystal approximation. The percolation model of the "one-bond and two mode" consideration developed for the long wave phonons in $Hg_{1-x}Cd_xTe$ is presented.

The experimental investigation of the $Hg_{1-x}Cd_xTe$ phonon spectra was undertaken by Kozyrev *et al.*[2] The composition dependence of the subtle structure of two subbands HgTe-like and CdTe-like observed were analyzed in detail and an interpretation in terms of based cells (tatrahadra) generating eight phonon modes, named canonical phonon modes (CPM) was presented. Nevertheless, the region below 118 cm^{-1} was excluded from consideration in Ref. 2. However several experiments indicated that in the range around 100–115 cm^{-1} additional lines[3–10] are located. There are important guiding principles that these lines are related to the defects.[6–10] This suggestion is presented too in another experimental work dedicated to the HgCdTe phonon spectra (see Ref. 7).

The MCT system is unique because the lattice mismatch is practically zero: from the EXAFS measurements[11] the nearest-neighbor bond lengths in the $Hg_{1-x}Cd_xTe$ crystals are found to be constant as a function of alloy compositions within experimental uncertainties 0.01 Å. It means that substitution of Hg-cation by Cd-cation does not give rise to the distinguished lattice deformations. On the other hand, the weak Hg-Te bond [introducing Cd-atoms to the lattice weaken this bond more in MCT (Ref. 12)] cause such self-defects as Hg-vacancy which are thermodynamically stable in the Hg-sublattice.[13]

It is known that far-infrared (FIR) spectra give direct information on phonon modes and impurity levels in the crystal lattices. Infrared spectroscopy enables us also to obtain information about their real crystalline microstructure and interior interactions.[14] If the intrinsic point defects or impurity defects are present in the ideal tetrahedron structure, additional frequencies, related to the specific properties of each defect appear in the optical spectra. Indeed, all such defects deform the ideal elemental tetrahedron described as a cation/anion at the center of a tetrahedron with four anions/cations at its vertexes. The size of the tetrahedron deformation depends on the kind of defects. Actually, the tetrahedron deformation modifies the electron charge distribution within the tetrahedron and consequently affects the distribution of the potential and of the field around all the constituents. The perturbation of the force field is responsible for the change in the vibrational spectra, with the appearance of new or modified frequencies due to local or resonant vibrational modes.[15–19] An additional mode caused by introducing the hydrogen atoms into the tetrahedra in the crystal lattice of CdTe was observed in the FIR-spectra, obtained using synchrotron radiation as source.[20] Therefore, FIR-spectra are very sensitive to disturbances of the crystal fields. The temperature dynamic of phonon spectra is exclusively important for the $Hg_{1-x}Cd_xTe$ system because the role of vacancies is

significant, as will be shown and the rise in temperature also means an increase of the vacancy concentration. This fact was noticed in Ref. 6 also where an influence of the temperature on the amplitudes and positions of lines were investigated for two compositions with the narrow gap of HgCdTe. In the case of the narrow gap when the phonon energy is comparable with the energy gap $E_g=\Gamma_6-\Gamma_8$ the returnable electron-phonon interaction can modify the phonon spectra.[21]

The FIR research cycle dedicated to the MCT system was performed in the wide temperature range for crystals of different types of conductivity (n and p type) and, as follows, from them- of different concentrations of Hg-vacancies. We used the synchrotron radiation as the light source which gives significant advantages, particularly for better spectral resolution. In an earlier short paper we showed[10] that the spectral lines at 100–115 cm^{-1} can be related to the Hg-vacancies. This hypothesis should be verified by the temperature dependences of the lines oscillator strengths discussed in the n- and p-type material. We will present in this paper the whole of the above mentioned results including the composition and temperature dependences as well as dependence on the Hg-vacancies concentration. Therefore, the temperature behavior of the phonon lines for some compositions of the HgCdTe alloys with different concentrations of Hg-vacancies will take a central place in this paper.

The paper consists of four sections. In the next section the experimental method and results will be described. The interpretation of experimental results obtained and a new hypothesis which explain these results will be presented in the third section and conclusions are formulated in the last section.

II. EXPERIMENT

A. Samples

The FIR spectra of nine $Hg_{1-x}Cd_xTe$ samples ($x=0.06-0.7$) were examined, produced by the liquid phase epitaxy (LPE). Special attention was given to samples of the identical $x=0.2$ composition, but of the different types of conductivity. In the case of the n-type sample the electron concentration obtained from the Hall effect measurements at the 77 K temperature is equal to 6.5×10^{13} cm^{-3} and in the case of the p-type sample the hole concentration is equal to 3.5×10^{15} cm^{-3}. It should be emphasized that electron mobility in the n-type sample was very high: $\mu=2.3\times10^5$ cm^2/Vs at 77 K.[21]

B. Experimental results

FIR reflectivity experiments were performed at the DAΦNE-light laboratory at Frascati (Italy) using the experimental setup described in Ref. 22. We used a BRUKER Equinox 55 FT-IR interferometer modified to collect spectra in a vacuum. As IR sources we used both the synchrotron radiation light emitted by the DAΦNE storage ring as well as a mercury lamp. The measurements were performed in the temperature range of 20–300 K and in the frequency range of 50–600 cm^{-1} at the spectral resolution of 1 cm^{-1} (2 cm^{-1} in some cases) collecting typically 200 scans within 600 s of acquisition time with a bolometer cooled down to 4.2 K. The reflectivity was measured by using as a reference a gold film evaporated onto the surface of the investigated samples. This method enabled us to measure the reflectivity coefficient with an accuracy of about 0.1%.[10,20]

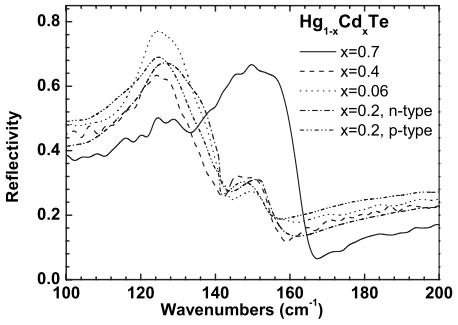

FIG. 1. Reflectivity spectra $Hg_{1-x}Cd_xTe$ (x is changing from 0.06 to 0.7) obtained at 300 K.

We calculated, similarly to earlier experiments (Refs. 10 and 21) from reflectivity spectrum, the imaginary part of the dielectric function $\mathrm{Im}[\epsilon(\omega,T)]$ by means of the Kramers-Kronig (KK) procedure with an estimated uncertainty of 5% for all experimental data.

The infrared reflectance spectra of the $Hg_{1-x}Cd_xTe$ alloys for compositions from $x=0.06$ to $x=0.7$ at the temperature 300 K and in the spectral range from 100 to 200 cm^{-1} are shown in Fig. 1. Two bands which shift weakly with the composition are observed: the first one around 118–130 cm^{-1} and the second around 140–160 cm^{-1}. The amplitude of the first band increases when the content of HgTe increases and amplitude of the second band increases when the CdTe content increases. The first band corresponds to the HgTe-like band and the second- to the CdTe-like band. This type of reflectance spectrum again shows, according to previous experiments[2,3,6] two-mode behavior of the optical phonons in the $Hg_{1-x}Cd_xTe$ alloys. Nevertheless the subtle structure at these two bands is clearly observed too, which confirmed the existence of more than two phonon modes for the MCT alloys, that were investigated in Ref. 2 and mentioned above as CPMs.

In Figs. 2 and 3 the reflectivity spectra for the n and p type of $Hg_{0.8}Cd_{0.2}Te$, respectively, in the temperature range 30–300 K are presented. These spectra show that the reflective maxima for the n-type MCT are more pronounced than for the p-type. For both types of samples, the peak maxima corresponding to HgTe-like optical phonon modes are shifted toward higher frequencies when the temperature rises, while the peak maxima corresponding to CdTe-like modes falls to lower frequencies as was found earlier.[7] We may also see on Figs. 2 and 3 additional lines on the lower frequency side.

The curves of the imaginary part of the dielectric function $\mathrm{Im}[\epsilon(\omega,T)]$ after Kramers-Kronig transformation of the reflectivity curves shown in Fig. 2 and 3, are presented in Figs. 4 and 5.

For n-type $Hg_{0.8}Cd_{0.2}Te$ the amplitude of the main HgTe-mode at 30 K is much higher and narrower than those for p-type $Hg_{0.8}Cd_{0.2}Te$. In Fig. 5 we can see considerable asym-

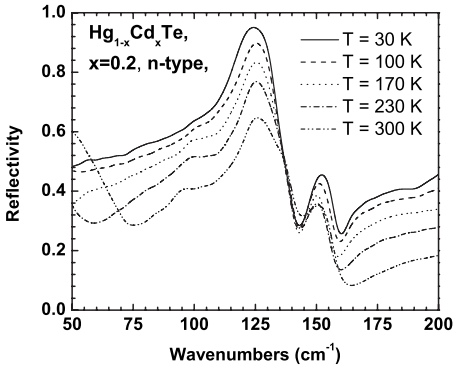

FIG. 2. Reflectivity spectra of the n-type $Hg_{0.8}Cd_{0.2}Te$ for the range 30–300 K

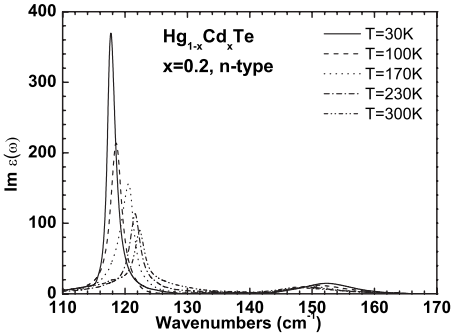

FIG. 4. Imaginary part of the dielectric function $Hg_{0.8}Cd_{0.2}Te$ n-type in the temperature range 30 K–300 K.

metry of HgTe-bands caused by additional lines in the range of 90 cm^{-1}–115 cm^{-1}. These are the additional lines, the origin of which has been discussed for the last three decades. The line amplitudes of CPMs (HgTe-like at 118–130 cm^{-1} as well as CdTe-like at 140–160 cm^{-1}) decrease when the temperature increases for both samples. Conversely, the line amplitudes of additional lines [we can call them additional phonon modes (APM)] increase when the temperature increases.

It is necessary to note from Figs. 4 and 5 that the shift of the HgTe-like band toward the higher frequency side with increase in temperature and the shift of the CdTe-like band to the lower frequency side when the temperature increases, are similar to results obtained in the work of Roth *et al.* (Ref. 7). The main TO-phonon mode frequency of HgTe-like band increases from 118 cm^{-1} at 30 K to 122.8 cm^{-1} at 300 K for the n type $Hg_{0.8}Cd_{0.2}Te$. In the case of the p-type sample a hardening of the HgTe-like TO mode from 118 to 121 cm^{-1} with an increase in temperature from 30 to 300 K is shown. We have inferred from the FIR-spectra that the signs of the temperature induced shifts of the HgTe-like and CdTe-like mode frequencies in the MCT alloy are opposite to each other for the composition range $x \leq 0.3$ which was noticed earlier (see Ref. 7). The CdTe-like mode frequency decreased from 153.7 to 151.5 cm^{-1} for n-type $Hg_{0.8}Cd_{0.2}Te$ and from 154.2 to 152 cm^{-1} for p-type $Hg_{0.8}Cd_{0.2}Te$ with an increase in temperature from 30 to 300 K. Simultaneously, the intensity of the HgTe-like and CdTe-like TO mode in both samples decreases and a higher background is observed for the p-type $Hg_{0.8}Cd_{0.2}Te$ in the spectral range 90–115 cm^{-1}.

C. Spectral analysis of the phonon bands of $Hg_{1-x}Cd_xTe$

The dispersion analysis of the main phonon bands (CPMs) and APMs was performed by approximating the $\mathrm{Im}[\epsilon(\omega,T)]$ curves by the Lorentzian sum,

$$\mathrm{Im}\ \epsilon(\omega) = \sum_{i=1}^{k} \frac{S_i \gamma_i \omega}{(\omega_{TOi}^2 - \omega^2)^2 + \omega^2 \gamma_i^2}, \qquad (1)$$

where S_i, ω_{TOi}, and γ_i are the oscillator strength, frequency and damping parameter of the i-phonon mode, respectively. This procedure was applied in our previous experiments concerning the phonon spectra of solid solutions.[10,20,21,23–25]

The results of spectral analysis for n- and p-$Hg_{0.8}Cd_{0.2}Te$ are presented in Figs. 6(a), 6(b), 7(a), and 7(b).

Parameters of Lorentzian's oscillators used for fitting the $\mathrm{Im}[\epsilon(\omega,T)]$-curves are shown in Tables I and II for the sample n-type $Hg_{0.8}Cd_{0.2}Te$ at the temperatures 30 K and 300 K and in Tables III and IV for the p-$Hg_{0.8}Cd_{0.2}Te$. In Tables II and IV the oscillator strengths sum for APM are shown separately as $(\Sigma S_{\mathrm{HgTe}})_{add}$.

It can be seen from Fig. 6(a) that the curve of the $\mathrm{Im}[\epsilon(\omega,T)]$ for n-$Hg_{0.8}Cd_{0.2}Te$ at 30 K may be approximated by the sum of the four Lorentzian's oscillators only. When

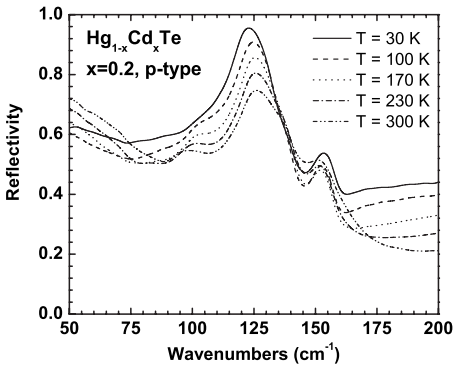

FIG. 3. Reflectivity spectra of the p-type $Hg_{0.8}Cd_{0.2}Te$ for the temperature range 30–300 K

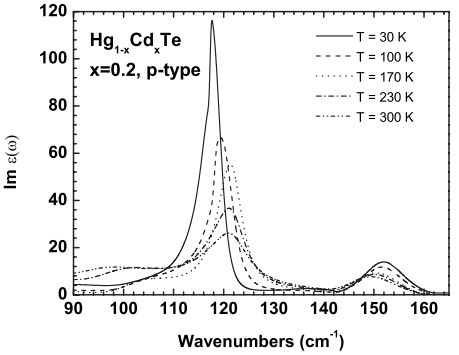

FIG. 5. Imaginary part of the dielectric function $Hg_{0.8}Cd_{0.2}Te$ p-type in the temperature range 30 K–300 K.

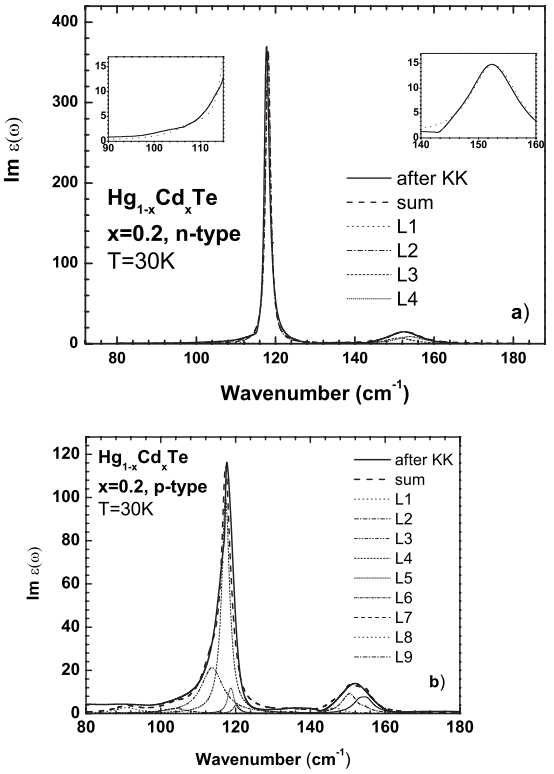

FIG. 6. Spectral analysis of the phonon bands of $Hg_{0.8}Cd_{0.2}Te$ *n*-type (a) and *p*-type (b) in the temperature 30 K: (a) for *n*-type, L1 to L4 Lorentzians which parameters are described in Table I; (b) for *p*-type L1-L8 Lorentzians which parameters are described in Table III.

the temperature increases to 300 K the two subbands of the $\mathrm{Im}[\epsilon(\omega,T)]$ curves observed are considerably wider [see Fig. 7(a)] and the number of the Lorentzians necessary for approximation at 300 K, increases to nine.

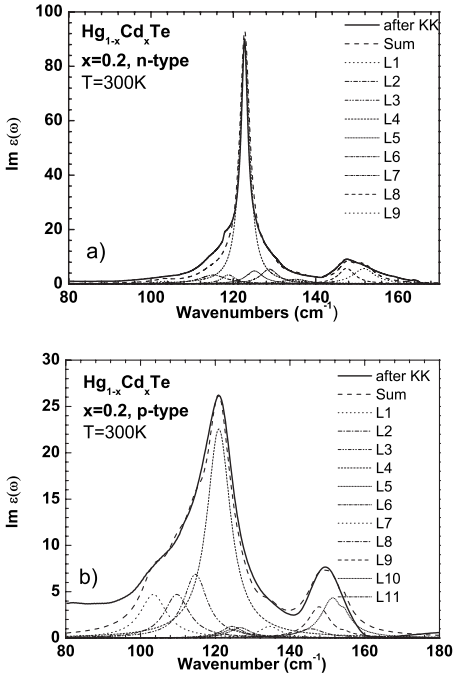

FIG. 7. Spectral analysis of the phonon bands obtained at the temperature 300 K, for *n*-type and *p*-type $Hg_{0.8}Cd_{0.2}Te$; the L1-L11 are the Lorentzians used for interpretation whose parameters are presented in Table I: (a) The spectra for *n*-type $Hg_{0.8}Cd_{0.2}Te$; (b) The spectra for *p*-type $Hg_{0.8}Cd_{0.2}Te$.

The analogous dissipation of the $\mathrm{Im}[\epsilon(\omega,T)]$ curves on the Lorentzians was carried out for the *p*-type $Hg_{0.8}Cd_{0.2}Te$ sample [see Fig. 6(b) and 7(b)]. The parameters of these oscillators are presented in Table III and IV.

There are eight well-resolved oscillators for *p*-type $Hg_{0.8}Cd_{0.2}Te$ at 30 K and eleven for this sample at 300 K. The positions of main HgTe-lines for *n*- and *p*-type are the same (118 cm^{-1}) at 30 K while the oscillator strengths of

TABLE I. Parameters of Lorentzian's oscillators used for fitting the $\mathrm{Im}[\epsilon(\omega,T)]$ curves of the *n*-$Hg_{0.8}Cd_{0.2}Te$ for the temperatures 30 K and 300 K.

Temperature (K)	Number of line	S (cm^{-2})	ω (cm^{-1})	γ (cm^{-1})	ΣS_{HgTe} CPM	ΣS_{HgTe} APM	ΣS_{CdTe} CPM	ΣS_{CdTe} APM
	1	<500	107	6.4		<500		
30	2	62500	118	1.35	62500			
	3	8400	151	7.7			19900	
	4	11500	153.7	8.4				
	1	500	103	5.0				
	2	3000	115	8.0		5100		
	3	1600	118.7	4.0				
	4	30800	122.6	2.8				
300	5	3000	125	5.0	37300			
	6	3500	128.6	5.0				
	7	1600	135	7.0				1600
	8	4000	147.3	4.7			9400	
	9	5400	151.5	6.3				

TABLE II. The specific oscillator's strength sums of the CPM and APM for n-$Hg_{0.8}Cd_{0.2}Te$ at 30 and 300 K.

Temperature (K)	$s^i_{HgTe}=\frac{S^i_{HgTe}}{\omega^2}$	$(\Sigma_j s^j_{HgTe})_{add}$
30	4.49	0.043
300	2.45	0.37

TABLE IV. The oscillator's sums of the CPM and APM for p-$Hg_{0.8}Cd_{0.2}Te$ at 30 and 300 K.

Temperature (K)	$s^i_{HgTe}=\frac{S^i_{HgTe}}{\omega^2}$	$(\Sigma_j s^j_{HgTe})_{add}$
30	3.44	0.5
300	1.54	1.19

these two lines are drastically different: 62 500 cm^{-1} for n-type and 48 000 cm^{-1} for p-type, respectively. The damping factor is nearly twice as large for p-type $Hg_{0.8}Cd_{0.2}Te$ because the line shape is more asymmetrical and wider in comparison to the n-type $Hg_{0.8}Cd_{0.2}Te$.

Additionally, the level of the background for the p-type $Hg_{0.8}Cd_{0.2}Te$ on the left side is essentially higher than for the n-type $Hg_{0.8}Cd_{0.2}Te$. When the temperature increases to 300 K the differences between n- and p-type $Hg_{0.8}Cd_{0.2}Te$ diminishes: the oscillator strengths of the main lines are 30 800 cm^{-2} and 21 100 cm^{-2}, respectively and the number of the Lorentzins increases to nine and eleven for n- and p-type HgTe-like subbands, respectively. We observed several additional lines in the range 90 to 115 cm^{-1} for both n- and p-type $Hg_{0.8}Cd_{0.2}Te$ at 300 K.

It is interesting to consider in detail the temperature behavior of the phonon modes observed for both n- and p-type $Hg_{0.8}Cd_{0.2}Te$. In Figs. 8 and 9 the temperature dependences of frequencies are shown for the phonon lines observed of the HgTe-like and CdTe-like subbands (CPMs) of n- and p-type samples. It can be seen that only one HgTe-like mode is observed at 30 K and two CdTe-like modes for n-$Hg_{0.8}Cd_{0.2}Te$ (see Fig. 8). When the temperature is higher than 100 K the splitting on the two HgTe-like modes takes place and finally at 300 K the three HgTe-like CPMs are displayed in the case of the n-type sample. Whereas in the region 90–115 cm^{-1}, one weak line is observed at 108 cm^{-1} whose amplitude increases with increase of temperature and after 230 K this line is split into three in the range 106–118 cm^{-1}.

The temperature dependencies of the phonon mode frequencies for p-$Hg_{0.8}Cd_{0.2}Te$ are presented in Fig. 9. We can see a considerably larger number of lines here in comparison with the n-type sample but the temperature shift of the phonon mode frequencies is similar.

These results obtained for the n- and p-$Hg_{0.8}Cd_{0.2}Te$ at 30 K agree generally with data presented in Refs. 2 and 7 but in these experiments a comparison for n- and p-type samples was not performed. Moreover, in previous experiments such a drastic difference between the phonon spectra of the n- and p-$Hg_{0.8}Cd_{0.2}Te$ was not shown. In the book by Dohrnhaus *et al.*[26] the reflectivity curves for n-$Hg_{0.8}Cd_{0.2}Te$ obtained at

TABLE III. Parameters of Lorentzian's oscillators used for fitting the $\mathrm{Im}[\epsilon(\omega,T)]$ curves of the p-$Hg_{0.8}Cd_{0.2}Te$ for the temperatures 30 and 300 K.

Temperature (K)	Number of line	S (cm^{-2})	ω (cm^{-1})	γ (cm^{-1})	ΣS_{HgTe} CPM	ΣS_{HgTe} APM	ΣS_{CdTe} CPM	ΣS_{CdTe} APM
	1	600	91	5				
	2	1500	107	4		6800		
	3	4700	112.4	4				
	4	48000	118	3.5	48000			
30	5	500	135	7				500
	6	1300	148	5				
	7	5800	151	5			15800	
	8	8700	154.2	6.2				
	1	4200	103.7	8.6				
	2	4200	110	8.1		14500		
	3	6100	115	7.7				
	4	21100	121.3	7.7				
300	5	830	125	7	23930			
	6	1000	127	7				
	7	1000	130	7				
	8	1200	135	7				1200
	9	1300	146.1	8.9				
	10	3500	148.3	7			9690	
	11	4890	152	7.4				

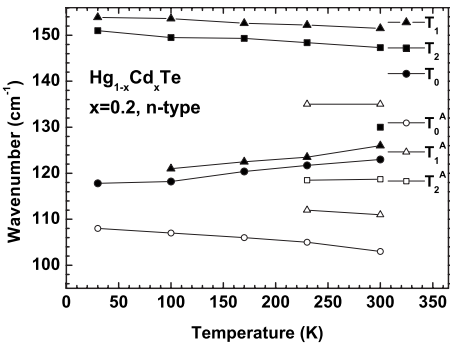

FIG. 8. The temperature dependencies of the phonon mode frequencies for n-$Hg_{0.8}Cd_{0.2}Te$ shown in Fig. 6(a) and Table I. T_0, T_1, and T_2 are tetrahedra generated the corresponding CPM modes. T_n^A are tetrahedra generated the corresponding APM modes.

30 and 300 K are presented. We transformed these reflectivity curves by the KK-procedure and the resulting $\mathrm{Im}[\epsilon(\omega,T)]$ curves are shown in Fig. 10. The resulting dispersion analyses are shown in Tables V and VI. It is clearly seen that these results are similar to our data obtained for p-$Hg_{0.8}Cd_{0.2}Te$ at 30 K (Fig. 9 and Tables III and IV). It means that the sample n-$Hg_{0.8}Cd_{0.2}Te$ for which reflectivity was measured presented in the book[26] contain a great number of the Hg-vacancies (conversion from p-type to n-type took place at high level of the Hg-vacancies). It is necessary to note that our sample of n-$Hg_{0.8}Cd_{0.2}Te$ was unique: very high electron mobility ($\mu=2.3\times10^5$ cm^2/Vs) and the resonance interaction of electrons with two phonons simultaneously was observed: the magnetophonon resonance on the difference of phonon frequencies.[27] This means a low level of the Hg-vacancy concentration at which a conversion from p to n type in the case of our n-type $Hg_{0.8}Cd_{0.2}Te$ occurred.

The analogous dispersion analyses were performed for all samples investigated of the $Hg_{1-x}Cd_xTe$ alloys, namely: with $x=0.06$ (p type), $x=0.28$ (n and p type), $x=0.40$ (p type), $x=0.70$ (p type). The aim of such research is to obtain the composition dependencies of the phonon mode frequencies including APMs.

The composition frequency dependencies for all phonon modes observed in the p-type MCT-system at the temperature of 300 K is presented in Fig. 11. It is seen that these dependencies are similar to those obtained in Ref. 2 but the APMs observed in the spectral region 104–116 cm^{-1} are presented here also. The amplitudes of these lines decrease with an increase of the CdTe-content.

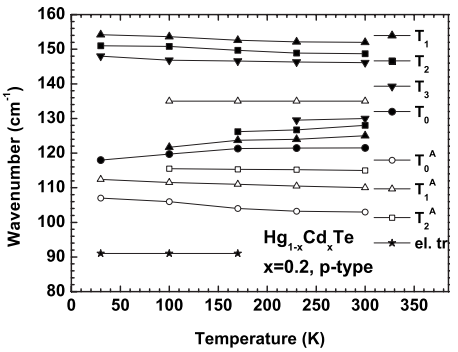

FIG. 9. The temperature dependencies of the phonon mode frequencies for the p-type $Hg_{0.8}Cd_{0.2}Te$, shown in Figs. 6(b) and 7(b) as well as in Table III. T_0, T_1, and T_2 are tetrahedra generated the corresponding CPM modes. T_n^A are tetrahedra generated by the corresponding APM modes.

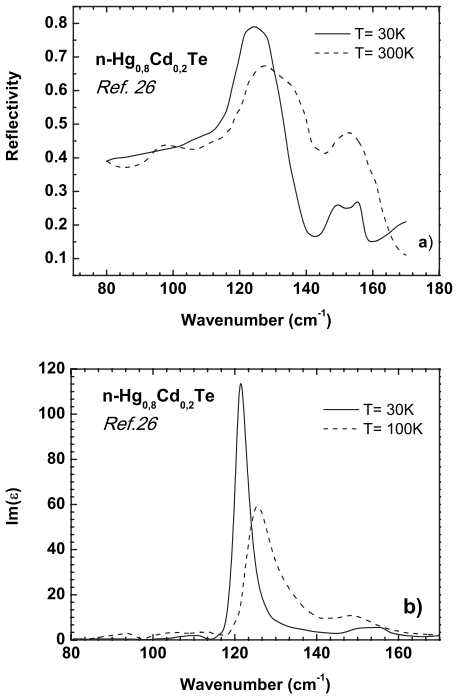

FIG. 10. Data on the phonon spectra of the n-type $Hg_{0.8}Cd_{0.2}Te$ from Ref. 26: (a) Reflectivity versus frequency, (b) Imaginary part of dielectric function obtained on base of the reflectivity spectra shown in Fig. 10(a).

These are the same lines for which temperature behavior was described above for the n and p type $Hg_{0.8}Cd_{0.2}Te$. Without doubt these lines are related to the HgTe-pairs oscillations. It is possible to state that the APMs reproduce the CPM of HgTe-like band but are shifted to lower frequencies.

III. DISCUSSION

A. General notes

The differences between the phonon spectra of the n- and p-$Hg_{0.8}Cd_{0.2}Te$ at 30 K [see Figs. 6(a) and 6(b)] are so large it seems that these two spectra belong to different materials. The dispersion analyses only (see Table I and III) show the same phonon frequencies for the main phonon modes (HgTe-like and CdTe-like) which means they are the same materials. The question requiring an answer is, what causes such great differences in the phonon spectra between materials of n and p type in the case of $Hg_{0.8}Cd_{0.2}Te$.

We would like to emphasize once more that the material n-$Hg_{0.8}Cd_{0.2}Te$ investigated is characterized by very high electron mobility. It should mean a low concentration of compensated acceptor centers—the Hg-vacancies. It could be a derived conclusion that it is necessary to distinguish the phonon modes of the low defect n-$Hg_{1-x}Cd_xTe$ from other $Hg_{1-x}Cd_xTe$ solid solutions because the latter include a great

TABLE V. Parameters of Lorentzian's oscillators used for fitting curves of the Imaginary part of dielectric function for the n-$Hg_{0.8}Cd_{0.2}T$ (Ref. 26) [see Fig. 10(b)].

Temperature (K)	Number of line	S (cm^2)	ω (cm^{-1})	γ (cm^{-1})	ΣS_{HgTe} CPM	ΣS_{HgTe} APM	ΣS_{CdTe} CPM	ΣS_{CdTe} APM
	1	500	110	4		500		
	2	610	117.5	4				
	3	44000	121.4	2.5	53510			
4.2	4	8900	125.4	5				
	5	2000	135	4				2000
	6	3000	151	4			7000	
	7	4000	155	6				
	1	710	112	6		1110		
	2	400	115.5	7				
	3	330	123	4				
	4	300	121.4	7	48630			
353	5	33000	125.6	5.1				
	6	15000	130	6				
	7	8100	135	8				8100
	8	7300	144	9				
	9	3000	149	5			16000	
	10	5700	153	8				

number of Hg-vacancies (the Hg-vacancies concentration).

It is possible to assume that the percolation theory presented in Ref. 1 is correct for close to the ideal solid solution. As was mentioned in the paper of Pages *et al.* (Ref. 1) "On the practical side, the percolation picture might renew interest in some zinc-blende mixed crystals, as multimode behavior in the Raman/infrared spectra is usually considered as abnormal, the result of rather poor crystalline quality or of nonrandom atomic substitution." Paradoxically, the percolation theory is confirmed (particularly at low temperature) for a more perfect n-type $Hg_{0.8}Cd_{0.2}Te$ crystal: at 30 K only one HgTe-like mode and two CdTe-like modes are observed (when temperature rises above 100 K we observed two or more HgTe-like modes). It is a necessary reminder that the lattice constants in HgTe and CdTe are practically the same (6.46 and 6.45 Å, respectively) therefore the crystals of these compounds mixed could be perfect (contains a low defect concentration).

The fact that there is frequency degeneracy of the four HgTe-like CPMs observed in the pure n-type $Hg_{0.8}Cd_{0.2}Te$ could be explained by this circumstance.

However the Hg-vacancies are always present in the $Hg_{1-x}Cd_xTe$ solid solutions with $x<0.7$ because they are thermodynamically stable in the lattice.[13] The question is whether the quantity of these vacancies is sufficient to attain such intensity of the phonon line which is observed in the experimental spectra (see Figs. 4–7) in the range of 104–116 cm^{-1}.

TABLE VI. The oscillator's sums of the CPM and APM for n-$Hg_{0.8}Cd_{0.2}T$ [26] At 4.2 and 300 K.

Temperature (K)	$s^i_{HgTe}=\frac{S^i_{HgTe}}{\omega^2}$	$(\Sigma_j s^j_{HgTe})_{add}$
4.2	3.54	0.45
353	2.13	0.85

B. Temperature dependencies of the specific oscillator strength sum

As mentioned in the Introduction, there are important guiding principles that the lines in the region 104–116 cm^{-1} are related to the Hg-vacancies. This hypothesis can be verified by temperature dependences of the specific oscillator strength sum (SOSS) of the lines observed in this region. These temperature dependences are presented in Fig. 12 for p-$Hg_{0.8}Cd_{0.2}Te$ and in Fig. 13 for n-$Hg_{0.8}Cd_{0.2}Te$.

It is shown in Fig. 12 that temperature dependency of the SOSS of APMs for p-type $Hg_{0.8}Cd_{0.2}Te$, have the exponential character described by the function,

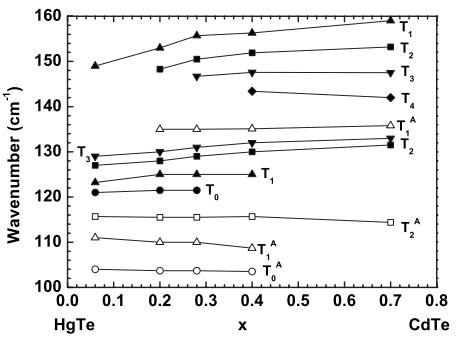

FIG. 11. The composition dependencies of the phonon mode frequencies for p-$Hg_{1-x}Cd_x$ Te, at temperature 300 K.

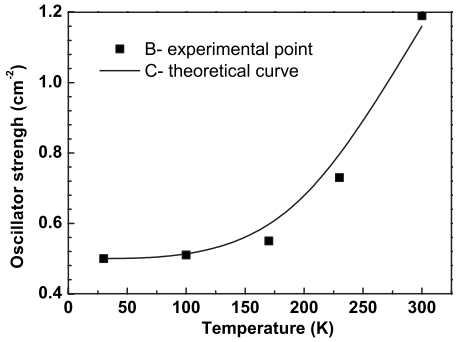

FIG. 12. The temperature dependence of the sum of the additional modes oscillator strengths for the *p*-type $Hg_{0.8}Cd_{0.2}Te$, B-experimental points, C is approximated curve calculated according the equation $s=0.5+12\ \exp(-0.075/\mathrm{kT})$.

$$\sum s^{add}_{\mathrm{HgTe}} = 0.5 + 12\ \exp(-0.075/kT) \tag{2}$$

with activation energy equal to 75 meV. It is too small an energy in comparison to the Hg-vacancy activation energy to be equal to about 1 eV.[13]

Figure 13 presents the temperature dependence of the SOSS of the same lines for *n*-type $Hg_{0.8}Cd_{0.2}Te$. This dependence is described by an exponential function similar to Eq. (2),

$$\sum s^{add}_{\mathrm{HgTe}} = 0.04 + 12\ \exp(-0.09/kT) \tag{3}$$

with activation energy equal to 90 meV, which is larger than for the *p* type but too small to be an activation energy for Hg-vacancies.

It is clear that the temperature dependencies of the SOSS of the lines observed in the region of 104–116 cm^{-1} do not confirm the hypothesis that these lines are related to the Hg-vacancies. There are other doubtful circumstances, namely: in the case of *n*-type $Hg_{0.8}Cd_{0.2}Te$ the single very weak line at 107 cm^{-1} is observed also at 30 K. If we assume that this line is caused by Hg-vacancies it is necessary to agree that the vacancy density must be not less than 10^{18} cm^{-3}. It is an absurdly great number of defects for a crystal with the electron mobility equal to 2.3×10^{5} $\mathrm{cm}^2/\mathrm{Vs}$.

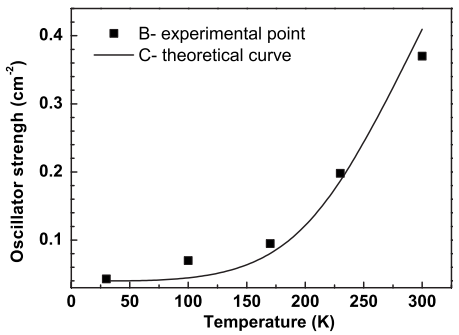

FIG. 13. The temperature dependence of the sum of the additional modes oscillator strengths for the *n*-type $Hg_{0.8}Cd_{0.2}Te$, C-experimental points, B is approximated curve calculated according the Equation $s=0.04+12\ \exp(-0.09/\mathrm{kT})$.

While the data of the positron annihilation for *n*-type HgCdTe (Ref. 28) shows values of the Hg-vacancy concentration rather closer to 10^{15} cm^{-3}, it is necessary to note that the positron annihilation seems to be a direct method of the vacancy concentration measurement.

However in the case of HgCdTe, this is incorrect because this method uses the Hall-effect to identify the hole concentration to the concentration of Hg-vacancies [$p=C_V^{Hg}$ for the model *p*-type HgCdTe (Ref. 28)]. In HgCdTe there is always a background of electrically native compensated Hg-vacancies and the real level of Hg-vacancies is naturally higher than the hole concentration. Nevertheless, the Hg-vacancy density over 10^{18} cm^{-3} in the *n*-$Hg_{0.8}Cd_{0.2}Te$ of high quality (very high electron mobility) is absolutely impossible.

In the case of *p*-type $Hg_{0.8}Cd_{0.2}Te$ the Hg-vacancy density is higher by two or three in the order of magnitude but it is difficult to assume that it can achieve the value of 10^{21} cm^{-3} (about a few molar percent which means that the density of Hg-vacancies should be the same as the density of the matrix atoms) as it results from the spectra shown in Figs. 6(b) and 7(b). This is also impossible.

Therefore, it is necessary to find a credible hypothesis which could explain the presence of lines in the range 104–116 cm^{-1} for HgTe and HgCdTe.

The temperature dependences of the SOSS for the lines discussed lead us to the activation energy of the process to be equal to 75–90 meV which could be a substantial argument for applying the model of two potential wells for Hg-atoms in the lattice of HgCdTe).[29,30]

C. Model of the two well potential for Hg-atoms in the lattice

Sussman[29] proposed this model for the binary compounds. According to this theory a cation in the crystal lattice could have two positions: the first stable position energetically deeper, the second is a metastable state with higher energy and suitably with a longer bond. This model related to HgTe and HgCdTe means that the Hg atoms can be shifted from the vertex position in a tetrahedra (stable position) to a noncentered position (metastable position). According to Sussman's theory[29] such transition from stable to metastable state, means that the Hg-Te bonds become longer. The probability for such transition is described by

$$W = w\ \exp(-\Delta E/kT), \tag{4}$$

where ΔE is the energy difference between the two states—stable and metastable (see Fig. 14) and w is the assumed probability at absolute zero.

The temperature dependences of SOSS for APM shown in Figs. 12 and 13 and described by the relationship (2) and (3) enable us to determine ΔE. Therefore, in the case of *p*-type $Hg_{0.8}Cd_{0.2}Te$ the energy transition from the stable position of the Hg atoms to the metastable position is 75 and 90 meV for the *n* type. This difference can be explained by the fact that for *p*-type material where a considerable part of the crystal lattice is nonrelaxed, the density of the metastable state is larger than in the *n*-type which could change the depth of the energy minimum (value E_2 see Fig. 14) for the stable posi-

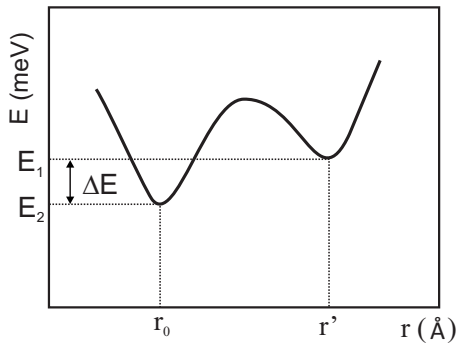

FIG. 14. Model of the two wells potential for Hg-atoms

tion. The ratio of the SOSSs of additional lines (104–116 cm^{-1}) for *p*- and *n*-type materials is about one order. Therefore, the density of the metastable and stable states should differ by the same value. Simultaneously, the length of the Hg-Te bonds is longer for the metastable states in comparison with the stable one. This difference can be noticed in x-ray analyses.

D. X-ray structural analysis

The x-ray diffraction spectra performed for the same *n*- and *p*-type $Hg_{0.8}Cd_{0.2}Te$ sample investigated in the far-infrared region are presented in Fig. 15(a) and 15(b). It is seen that they demonstrate essential differences in both position and form of the diffraction maxima.

The diffraction maximum corresponding to (111) face [Fig. 15(a)] have different positions for *n*- and *p*-type materials, namely: $2\Theta=23.811°$ and $2\Theta=23.275°$, respectively.

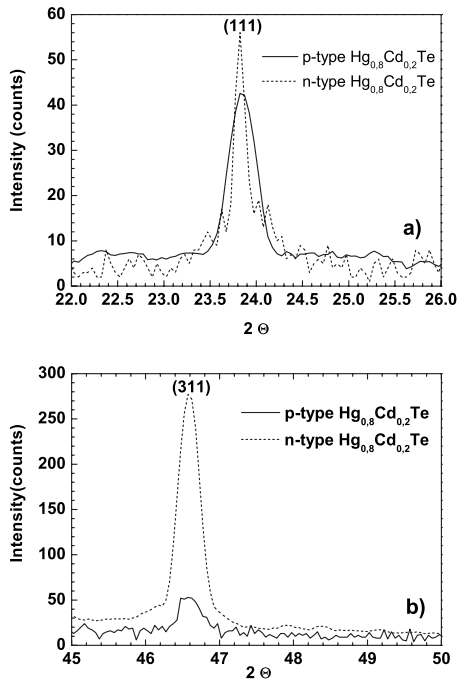

FIG. 15. Diffraction x-ray spectra $Hg_{0.8}Cd_{0.2}Te$ at 300 K, (a) comparison (111) peaks for n and *p*-type $Hg_{0.8}Cd_{0.2}Te$, (b) comparison (311) peaks for *n* and *p*-type $Hg_{0.8}Cd_{0.2}Te$.

This maximum is broad for the *p* type and sharp for the *n*-type material. The lattice constants derived from the diffraction maximum positions are: 6.4604 and 6.4648 Å, for *n* and *p* type, respectively.

The data concerning these two samples of $Hg_{0.8}Cd_{0.2}Te$ are collected in Table VII. We can see that in the high quality *n*-$Hg_{0.8}Cd_{0.2}Te$ crystal the lattice constant is less than in the *p*-type. It means that the crystal lattice for the *p*-$Hg_{0.8}Cd_{0.2}Te$ is more swollen. A considerable number of Hg-atoms were introduced in the lattice of the *n*-type material at the annealing process in the Hg-vapor atmosphere. While in the case of the *p*-type material (as grown) there are a great number of the Hg-vacancies which result in lattice strain and favor the metastable positions of the Hg-atoms in the lattice with longer bond length. In the *n*-type lattice the strains are relaxed during the long annealing process and the overwhelming majority of the Hg-atoms occupy the stable positions with shorter bond length.

Therefore, the x-ray structural analyses confirmed our hypothesis that in the case of *n*-type material the majority of the Hg-atoms occupy the stable position in the lattice. It is not obvious for all *n*-$Hg_{0.8}Cd_{0.2}Te$ samples.

In Figs. 10(a) and 10(b) and Table V data for *n*-$Hg_{0.8}Cd_{0.2}Te$ taken from Ref. 26 are presented, where no great differences in comparison with *p*-type material were observed. This fact means that the donor concentration obtained by these authors are in excess at the high level of the Hg-vacancy concentration—considerably higher than in our *n*-type $Hg_{0.8}Cd_{0.2}Te$ and that the lattice in this "weak" *n*-type $Hg_{0.8}Cd_{0.2}Te$ is not relaxed and the phonon spectrum is closer to the *p*-type material. This same one concern is in the work of Amirtharaj *et al.*[6]

In Fig. 15(b) the x-ray diffraction maximum for the plane (311) is shown which indicates the degree of the lattice ordering. In the case of *n*-type $Hg_{0.8}Cd_{0.2}Te$ this maximum is many times sharper and higher than for *p*-type $Hg_{0.8}Cd_{0.2}Te$. It confirms the assumption about the comparably high quality and stable crystal lattice for our *n*-$Hg_{0.8}Cd_{0.2}Te$.

E. General description of the phonon spectra in the HgCdTe alloys

The general description of the phonon spectra is based on three figures: Figs. 9–11. These figures present the temperature dependences of the HgTe-like and CdTe-like mode frequencies for *n*- and *p*-type $Hg_{0.8}Cd_{0.2}Te$ (Fig. 9 and 10) as well as the composition dependences of the same modes at room temperature (Fig. 11). If temperature increases, the number of Hg-atoms occupying the metastable positions (Hg^{II}) increases also and the deformation of crystal lattice rises. The last factor should cause the removal of degeneracy of the HgTe-like CPMs in *n*-$Hg_{0.8}Cd_{0.2}Te$ when the temperature increases to over 100 K (see Fig. 9); the APMs appear simultaneously, too. Indeed, the APM at 112 cm^{-1} (as well as very weak APM starting at 30 K at 108 cm^{-1}) takes place above 100 K in the *n*-type $Hg_{0.8}Cd_{0.2}Te$ and over 200 K additionally another APM at 104–116 cm^{-1} appears. The presence of Hg^{II} in a tetrahedron leads to the stretching of bonds which in turn causes the shift of the Hg-Te oscillation

TABLE VII. The parameters of the $Hg_{0.8}Cd_{0.2}Te$ crystals.

Type of conductivity	Carrier mobility (77) (m^2/Vs)	ΔE-the activation energy of the SOS-temperature dependence, meV	Position of the diffraction maximum (111)-2Θ, degree	Lattice constant(Å)
n-type	2.3×10^5—electrons	90	23.811	6.4604
p-type	3.5×10^3—holes	75	23.275	6.4648

frequency toward smaller frequencies. This effect can occur in three kinds of tetrahedra: (1) containing three Hg-atoms in the stable position (Hg^I) and one Hg^{II}; (2) containing two Hg^I, one Cd-atom and one Hg^{II}; (3) containing one Hg^I, two Cd-atoms and one Hg^{II}. The frequencies of Hg-Te oscillations in these three type of tetrahedra should be arranged in the following sequence: the lowest frequency corresponds to the Hg-Te oscillations in the tetrahedron of the first type and the highest corresponds to the oscillations in the tetrahedron of the third type.

The lines in the range of 135–137 cm^{-1} are generated as could be assumed, by the oscillation of the Cd-Te pair in the tetrahedra containing two Hg^I, one Cd-atom and one Hg^{II}.

Therefore, Figs. 9–11 enable us to assume that the phonon spectra in the MCT are reproduced in two versions: the first one is realized in the lattice consisting only from the Hg^I-atoms (that are CPM) and the second one occurs in the lattice including the Hg^{II}-atoms (that are APM).

The theory of the quasiquaternary alloys containing the two kinds of Hg-atom positions developed in Ref. 10 enable us to determine the Hg^{II} concentration on the basis of phonon spectra. The details of this consideration are presented in the Appendix. Arising from Eqs. (A1)–(A5) the sum of the specific oscillator strengths of APM in the range 104–116 cm^{-1} is equal to

$$S^{\mathrm{HgTe}}_{n,\mathrm{Hg}^{II}}(y) = f_{\mathrm{HgTe}}y. \tag{5}$$

This simple expression enables us to determine experimentally (using the phonon spectra) the *y*-molar part of the Hg^{II} atoms, assuming that: (i) the lines corresponding to the APM generated by the tetrahedra bearing Hg^{II} are identified correctly, (ii) the specific oscillator strength of the Hg^{II}-Te oscillations in the tetrahedra with Hg^{II} atoms are the same as for the Hg-Te oscillators. We assume that these conditions are fulfilled in the case of the materials measured of *n*- and *p*-type $Hg_{0.8}Cd_{0.2}Te$. The calculated values of the molar fraction *y* of the Hg^{II}-Te obtained from the phonon spectra (sum of the specific oscillator strength) are presented in Table VIII for 30 and 300 K.

It is necessary to note that such a large concentration of Hg^{II} in the case of *p*-type $Hg_{0.8}Cd_{0.2}Te$ conducts a considerable deformation of the lattice, which completely removes the CPM frequency degeneration and above 200 K we observed four HgTe-like canonical modes (Fig. 9). On the other hand, the considerable deformations of the lattice appear in the x-ray diffraction of *p*-$Hg_{0.8}Cd_{0.2}Te$ as was observed, see Figs. 15(a) and 15(b) and lead to an increase of the lattice constant and blur the (311) diffraction maximum.

IV. CONCLUSION

The phonon spectra of $Hg_{1-x}Cd_xTe$ in the wide temperature range (30–300 K), the composition (from $x=0.06$ to $x=0.7$) and Hg-vacancy concentration has been studied. The temperature dependencies of the phonon frequencies and the sum of the oscillators strengths of various kinds of phonon modes (HgTe-like and CdTe-like) for *p*- and *n*-type $Hg_{0.8}Cd_{0.2}Te$ crystals have considerable differences. This could be shown by the significant contribution of the Hg-vacancies in the phonon spectra because the main difference between *p* and *n* type of $Hg_{1-x}Cd_xTe$ lattices is the huge number the Hg-vacancies in the *p*-type material, as mentioned in our previous work.[10] However the assumption that such strong intensity of the APM-lines discussed is caused by the tetrahedra with the mercury vacancies cannot be accepted.

It seems that the two valley model of the potential for the mercury atom in the HgCdTe lattice is the more realistic hypothesis.[29,30] The temperature dependences of the sums of the oscillator strengths for AVP in the range 104–116 cm^{-1} for *n*- and *p*-type HgCdTe shows the activation energy 90 and 75 meV, respectively, which corresponds to the transition energy of the mercury atoms from the deeper minimum (stable) to second minimum (metastable).

It is necessary to assume that the density of the Hg-metastable states in a lattice is about 10% of the whole number of Hg-atoms in the *p*-$Hg_{1-x}Cd_xTe$. The long-time annealing of HgCdTe at 220 °C (inversion to the *n* type) leads to the relaxation of the lattice and reversion of Hg atoms to the stable state. The data of x-ray structure analyses confirms this hypothesis.

With this assumption, we can affirm that in the case of the *p*-type crystals the HgCdTe-lattice consists of two coexisting and penetrating sublattices: one sublattice contains the atoms of mercury in the stable state with the shorter length bonds of Hg-Te; the second sublattice contains the Hg atoms in the metastable state with the longer bond of Hg-Te.

TABLE VIII. Molar fraction of the Hg^{II}-atoms determine from phonon spectra.

	Sum of the specific oscillator strength for APM		*y*, mol. %	
Material	30 K	300 K	30 K	300 K
n-type $Hg_{0.8}Cd_{0.2}Te$	<0.043	0.37	<0.7	6.3
p-type $Hg_{0.8}Cd_{0.2}Te$	0.50	1.1987	9.7	20.67

The phonon spectra of MCT are reproduced for each sublattices mentioned. Increase in temperature leads to the growth of the Hg-atom number in the metastable state and simultaneously to the enlargement of the Hg-Te bonds (tensions in the lattice) which leads to the frequency splitting of the HgTe-like CPMs in the *n*-type material. Due to this the differences between the phonon spectra of the *n*- and *p*-type HgCdTe disappear at room temperature.

Increase of the content of CdTe in the HgCdTe crystal leads to the same effect as an increase in temperature: i.e., results in the increase of the number of the CPMs (to the frequency splitting for both HgTe-like and CdTe-like modes). This takes place because the content of the mercury atoms in the metastable state increases and due to the enlargement of the Hg-Te bonds (increase tensions in the crystalline lattice) the degeneracy of the CPMs is removed.

One can affirm that at temperature 30 K the degeneracy of CPMs takes place in the *n*-type $Hg_{0.8}Cd_{0.2}Te$ and HgTe-like mode as well as two CdTe-like modes. This would be confirmation of the percolation theory of Pages.[1]

APPENDIX

As discussed in the introduction, the $Hg_{1-x}Cd_xTe$ crystals are characterized by the basic tetrahedra, each with a central ion surrounded in the first coordination shell by its four nearest neighbors (NN) at the vertices. Verleur and Barker,[31] studying the $GaAs_yP_{1-y}$ system, explained the vibrational spectra of a ternary solid solution in terms of five basic elemental tetrahedra. In the $A_xB_{1-x}Z$ ternary tetrahedral structures several tetrahedron configurations T_n (n is the number of B atoms in the tetrahedron) coexist simultaneously: 2 strictly-binary corresponding to the AZ and the BZ compounds whose lattices are characterized by the tedrahedral units T_0 and T_4 (configurations) respectively, and 3 strictly-ternary, i.e., characterized by the configurations T_1, T_2, and T_3. In an ideal crystal lattice they all together generate at least $(2\times1)+(3\times2)=2+6=8$ optically active phonon modes. Thus, eight different lines could be observed in the experimental phonon spectra as a subtle structure of two bands, AZ-like and BZ-like. These are the CPMs some of which, as was mentioned above, appeared as fine structures of two bands lying in the ranges 118–135 cm^{-1} (HgTe-like CPMs) and 140–160 cm^{-1} (as CdTe-like CPMs).

In the crystalline ternary alloys $Hg_{1-x}Cd_xTe$ as was shown in subchapter III.5 two positions of Hg-atoms are possible in the crystalline lattice: a thermodynamically stable (Hg^I) and metastable (Hg^{II}). These crystals containing two positions of the Hg-atoms cannot be described as an ideal ternary alloy $A_xB_{1-x}Z$ (x is the molar fraction of A atoms) because the essential properties will not be included in this consideration. It is useful to apply a model of quasiquaternary alloy $(A_xB^I_{1-x-y}B^{II}_y)Z$,[10] where y is the fraction of the B^{II} atoms (abnormal position in lattice) while the fraction of B^I atoms (normal position in lattice) will be $1-x-y$ where x is the fraction of A atoms. Consequently, an additional configuration T_nHg^{II} now appears in the lattice (here we ignore the possibility of having two Hg^{II} simultaneously in a tetrahedron because an eventual contribution due to multiple metastable positions per tetrahedron is below the sensitivity of our method). Actually, there are three of these "strictly quaternary" configurations: $T_{3Hg^{II}}, T_{2Hg^{II}}$ and $T_{1Hg^{II}}$ including respectively, 3, 2, and 1 A atoms (Cd cations) and respectively 0, 1, and 2 B^I atoms (Hg^I) contributing, together with three additional HgTe-like modes and two additional AZ-like (CdTe-like) modes to the phonon spectrum. We must assume that the frequencies of Hg-Te oscillations in the Hg^{II}-bearing tetrahedra and in the Hg^{II} free tetrahedra are different. According to the Bernoulli distribution the populations of each of the "strictly quaternaries" or Hg^{II}-bearing tetrahedra are proportional to the probability of identifying the corresponding $T_{n,m}$ configuration in the lattice. The probability of finding an Hg^{II}-atom in the $T_{n,m}$ configuration in the lattice is[32]

$$P^{Hg^{II}}_{nm}(x,y)=\frac{m}{4}\binom{4-n}{m}\binom{4}{n}x^n y^m(1-x-y)^{1-n-m}, \qquad \text{(A1)}$$

where m is the number of the Hg^{II}-atoms in a tetrahedron ($m=1$ in our case) and n is the number of Cd-atoms in the $T_{n,m}$ configuration. The latter is also identified as $T_{nHg^{II}}$. The oscillator strength of the vibrational mode generated by a Hg^{II}-Te-dipole in the configuration is (Ref. 2)

$$S^{Hg-Te}_{n,Hg^{II}}(x,y)=f_{Hg-Te}NP^{Hg^{II}}_{n,Hg^{II}}(x,y), \qquad \text{(A2)}$$

where the oscillator strength of the single dipole Hg-Te-pair $f_{Hg\text{-}Te}$ is equal to 5.8 at 77 K,[26] and N is the total number of cations (or inion pairs) in the alloy per unit value.

In this analysis we do not include the factor relating to the site-occupation preferences of atoms (SOP) in the tetrahedra which leads to a nonrandom distribution of basic cells in the lattice.[33] The influence of SOP as well as other effects, such as the electron-phonon interaction or relativistic effects, important for this class of materials, will be considered in the next paper dedicated to low-defected crystals.

For HgCdTe ideal lattices four HgTe-like CPMs and four CdTe-like CPMs contribute to the sum in the Eq. (1) (Sec. II and III). Within this approximation the experimental $\mathrm{Im}[\epsilon(\omega,T)]$-curves allow one to find the s_i values. If the role of defects is negligible, the oscillator sum rule

$$\begin{aligned}\sum_n S^{HgTe}_n(x)&=\sum_n f_{HgTe}NP^{Hg}_n(x)\\&=f_{HgTe}N\sum_n P^{Hg}_n(x)\\&=f_{HgTe}(1-x)\end{aligned} \qquad \text{(A3)}$$

has to be satisfied. Therefore the sum of the oscillator strengths of the AZ or BZ mode has to be proportional to the molar fraction of the AZ or BZ components. In Ref. 2 Kozyrev *et al.* showed that this rule is not fulfilled in HgCdTe alloys and additional contributions have to be taken into account. The modes generated by Hg^{II}-bearing tetrahedra described by the oscillator strength of Eq. (A2) should be included in the sum of Lorentzians in Eq. (1). The additional terms should improve the agreement with the experimental data for the $\mathrm{Im}[\epsilon(\omega,T)]$ and restore the correct oscillator strength sum of a quasiquaternary alloys

$$\sum S_{n,m}^{\mathrm{HgTe}} = f_{\mathrm{HgTe}}(1-x-y) + f_{\mathrm{HgTe}}(y) \equiv f_{\mathrm{HgTe}}(1-x), \tag{A4}$$

At the same time the sum in Eq. (A4) consists of two terms

$$\sum S_{n,m}^{\mathrm{HgTe}} = \sum S_{n}^{\mathrm{HgTe}}(1-x-y) + \sum S_{n,\mathrm{Hg}^{II}}^{\mathrm{HgTe}}(y), \tag{A5}$$

where the first term describes the HgTe-like subband in the range of 118–135 cm^{-1} due to CPMs and the second one, the HgTe-like subband in the range 104–116 cm^{-1} containing the APM associated with Hg^{II}. The Eq. (A5) enables us to describe quantitatively the subbands observed experimentally in the FIR spectra of HgCdTe solid solutions and to calculate the y-molar fraction of the Hg^{II} atoms.

*sheregii@univ.rzeszow.pl

[1] O. Pagès, T. Tite, K. Kim, P. A. Graf, O. Maksimov, and M. C. Tamargo, J. Phys.: Condens. Matter **18**, 577 (2006).
[2] S. P. Kozyrev, L. K. Vodopyanov, and R. Triboulet, Phys. Rev. B **58**, 1374 (1998).
[3] J. Baars and F. Sorgers, Solid State Commun. **10**, 875 (1972).
[4] S. C. Shen and J. H. Chu, Solid State Commun. **48**, 1017 (1983).
[5] D. N. Talwar, J. Appl. Phys. **56**, 1601 (1984).
[6] P. M. Amirtharaj, N. K. Dhart, J. Baars, and H. Seelewind, Semicond. Sci. Technol. **5**, S68 (1990).
[7] S. Rath, K. P. Jain, S. C. Abbi, C. Julien, and M. Balkanski, Phys. Rev. B **52**, 17172 (1995).
[8] Li. Biao,J. H. Chu, H. J. Ye, S. P. Guo,W. Jiang, and D. Y. Tang, Appl. Phys. Lett. **68**, 3272 (1996).
[9] J. Polit, E. M. Sheregii, J. Cebulski, M. Pociask, A. Kisiel, A. Mycielski, E. Burattioni, A. Marcelli, M. Castelli Guidi, M. Piccinini, P. Calvani, and A. Nucara, Eur. Phys. J. Appl. Phys. **27**, 321 (2004).
[10] J. Cebulski, E. M. Sheregii, J. Polit, A. Marchelli, M. Piccinini, A. Kisiel, I. V. Kucherecho, and R. Triboulet, Appl. Phys. Lett. **92**, 121904 (2008).
[11] R. A. Mayanovic, W. F. Pong, and B. A. Bunker, Phys. Rev. B **42**, 11174 (1990).
[12] A. Sher, A. B. Chen, W. E. Spicer, and K. Shih, J. Vac. Sci. Technol. A **3**, 105 (1985).
[13] D. Chandra, H. F. Schaake, J. H. Tregilgas, F. Aqariden, M. A. Kinch, and A. J. Syllaios, J. Electron. Mater. **29**, 729 (2000); D. Chandra, H. F. Schaake, and M. A. Kinch, *ibid.* **32**, 810 (2003).
[14] B. V. Robouch, A. Kisiel, and E. M. Sheregii, Phys. Rev. B **64**, 073204 (2001).
[15] A. Maradudin, *Theoretical and Experimental Aspects of the Defects and Disorder on the Vibrations in Crystals*, Solid State Physics, edited by H. Ehrenreich (Academic, New York, 1966), Vols. 18 and 19.
[16] S. S. Mitra, *Vibration Spectra of Solids*, Solid State Physics, edited by H. Ehrenreich (Academic, New York, 1962), Vols. 13.
[17] A. S. Barker and J. Sievers, Rev. Mod. Phys. **47**, S1 (1975).
[18] R. C. Newman, in *Semiconductors and Semimetals* (Academic Press, New York, 1993), Vol. 38, pp. 117–187.
[19] A. M. Kossevich, *The Crystal Lattice* (Wiley-VCH, Berlin; NewYork, 1999).
[20] J. Polit, E. M. Sheregii, J. Cebulski, B. V. Robouch, A. Marchelli, M. Cestelli Guidi, M. Piccinini, A. Kisiel, P. Zajdel, E. Burattini, and A. Mycielski, J. Appl. Phys. **100**, 013521 (2006).
[21] E. M. Sheregii, J. Cebulski, A. Marcelli, and M. Piccinini, Phys. Rev. Lett. **102**, 045504 (2009).
[22] M. Cestelli Guidi, M. Piccinini, A. Marcelli, A. Nucara, P. Calvani, and E. Burattini, J. Opt. Soc. Am. A **22**, 2810 (2005).
[23] J. Polit, E. M. Sheregii, J. Cebulski, B. V. Robouch, A. Marchelli, M. Cestelli Guidi, M. Piccinini, and A. Kisiel, Infrared Phys. **49**, 23 (2006).
[24] J. Cebulski, E. M. Sheregii, J. Polit, A. Kisiel, B. V. Robouch, A. Marchelli, M. Cestelli Guidi, and M. Piccinini, Infrared Phys. **49**, 19 (2006).
[25] E. M. Sheregii, J. Polit, J. Cebulski, A. Kisiel, B. V. Robouch, A. Marchelli, M. Cestelli Guidi, and M. Piccinini, Infrared Phys. **49**, 13 (2006).
[26] R. Dornhaus and G. Nimitz, Solid State Phys. **78**, 1 (1976).
[27] E. M. Sheregii, Yu. O. Ugrin, and D. D. Shuptar, JETP Lett. **47**, 711 (1988).
[28] R. Krause, A. Klimakow, F. M. Kiessling, A. Polity, P. Gille, and M. Schenk, J. Cryst. Growth **101**, 512 (1990).
[29] J. A. Sussmann, J. Phys. Chem. Solids **28**, 1643 (1967).
[30] S. P. Kozyrev, Phys. Solid State **35**, 865 (1993).
[31] H. W. Verleur and A. S. Barker, Phys. Rev. **149**, 715 (1966).
[32] J. M. Ziman, *Models of Disorder* (Cambridge University Press, Cambridge, England, 1979).
[33] B. V. Robouch, A. Kisiel, and J. Konior, J. Alloys Compd. **339**, 1 (2002).